

Structured Illumination in Spatial-Orientational Hyperspace

Karl Zhanghao^{1,*†}, Xingye Chen^{2,*}, Wenhui Liu², Meiqi Li¹, Chunyan Shan³, Xiao Wang⁴, Kun Zhao¹, Amit Lai¹, Hao Xie², Qionghai Dai^{2,†}, Peng Xi^{1,†}

¹ Department of Biomedical Engineering, College of Engineering, Peking University, Beijing 100871, China

² Department of Automation, Tsinghua University, Beijing 100084, China

³ Department of Life Sciences, Peking University, Beijing 100871, China

⁴ Center for Life Sciences, Peking University, Beijing 100871, China

* These authors contributed equally to this work.

† Correspondence: P.X. (xipeng@pku.edu.cn), Q.D. (daiqh@tsinghua.edu.cn), K.Z. (karl.hao.zhang@gmail.com)

The dipole nature of chromophore is important for both super-resolution microscopy and imaging molecular structure, which is nevertheless neglected in most microscopies, even including structured illumination microscopy (SIM) with polarized excitations. Here we interpret fluorescent dipoles in spatial-orientational hyperspace, in which polarized excitation is structured illumination on the dimension of dipole orientation. Furthermore, we developed polarized SIM (PSIM), which attains super-resolution imaging of fluorescent dipoles directly on commercial SIM systems.

Both the absorption and emission process of chromophores are polarization sensitive, physically termed as dipoles. The dipole model plays an important role in super-resolution microscopy. Considering polarized emission, the localization accuracy of single molecular imaging could be improved[1]. With polarization modulated excitation, super-resolution imaging could be obtained by demodulation algorithm with regular labeling strategies[2, 3, 4]. When targeted to biological structures, the fluorescent dipole connects its polarization with the molecular structure of the specimen. For example, G-protein activation on cell membrane could be measured by two-photon polarization microscopy[5]. Structural understanding of macromolecules such as nuclear pore complex[6], ATPase[7] and myosin[8] are improved by various fluorescent polarization microscopy (FPM). Biological filaments, such as actin, septin, and DNA filament, usually behave with strong polarization, which is widely studied by FPM[9, 10, 11, 12]. Despite that most fluorescent tags exhibit dipole effect, it is seldom employed in many microscopic techniques. Interestingly, even the rotational polarized excitation is employed in SIM (Figure 1b), the dipole feature of the specimen is still neglected.

To provide a universal framework for considering polarization in microscopy, we interpret the sample in spatial-orientational hyperspace or x - y - α coordinate, by stretching the dipoles on an additional dimension of orientation. Figure 1a illustrates dipoles of the specimen on x - α section. When excited by polarized light, the dipoles are structurally illuminated on orientational dimension: the ones parallel to the polarization have largest absorption efficiency while the ones perpendicular are not excited at all. The quantitative relationship between absorption efficiency and dipole orientation is also a sinusoidal function, analogous to spatial structured illumination (Eq. 1). Fourier transform of the sinusoidal pattern contains three frequency components. With polarization modulation, or changing the phases of orientational structured illumination, these frequency components could be solved separately. In this way, higher frequency orientational information could be observed, enabling measurement of dipole orientation. At least three polarized excitations are required, which

is consistent with fitting the dipole orientations from their polarization response as used in linear dichroism[12, 13]. Nonlinear polarized excitation could generate more frequency components on orientation axis, further improving orientational resolution. For example, Two-photon excitation (TPE)[5] and Excitation Polarization Angle Narrowing (ExPAN)[2] are two types of nonlinear polarized excitation studied in previous research (Figure S1). When second or higher harmonic frequencies are acquired, multiple dipoles at the same position or the wobbling behavior of dipoles may be resolved. A system with polarized detection is able to measure dipole orientation by itself. When combined with polarized excitation, polarized detection allows to measure an additional harmonic of orientational frequency (Figure S2). We also use a combination of linear polarized excitation and polarized detection to measure the illumination pattern of nonlinear SIM in the following context.

$$\begin{aligned}
\text{polarizedexcitation} : \quad & F_\theta(\alpha) = \frac{\eta}{2}[1 + \cos(2\pi \cdot \frac{1}{\pi}\alpha - 2\theta)] \\
\text{structuredillumination} : \quad & I_{\theta,\phi}(\mathbf{r}) = \frac{I_0}{2}[1 + \cos(2\pi\mathbf{k}_\theta \cdot \mathbf{r} + \phi)] \\
\text{SIM} : \quad & D = [S_p(\mathbf{r}, \alpha) \cdot I_{\theta,\phi}(\mathbf{r}) \cdot F_\theta(\alpha)] \otimes PSF
\end{aligned} \tag{1}$$

where $F_\theta(\alpha)$ denotes the polarized excitation in orientational dimension with the polarized of θ , $I_{\theta,\phi}(\mathbf{r})$ denotes structured illumination in spatial dimensions with pattern θ and phase ϕ , D denotes the detected image, $S_p(\mathbf{r}, \alpha)$ denotes the sample information in the reciprocal space and PSF denotes the point spread function of the system.

Spatial-orientational hyperspace shows more advantage over fitting polarization response when it comes to SIM. SIM generates both spatial structured illumination by interference and orientational structured illumination by polarized excitation (Eq. 1). Taken the direction of k vector as x -axis which is perpendicular to the illumination pattern, we could display the spatial-orientational structured illumination in x - α coordinate (Figure 1c). The spatial-orientational pattern of structured illumination contains higher frequency components on all dimensions after Fourier transform (Figure 1e). It actually doubles both spatial resolution and orientational resolution. To verify spatial-orientational structured illumination, uniformly distributed 20-nm fluorescent beads are excited under polarized structured illumination and imaged. The fluorescent beads are known as polarization isotropic or have uniform distribution on orientational axis. However, they behave polarized response under polarized excitation, which are measured by polarized detection. Then the images are rotated to have k vector as x -axis and displayed in x - α coordinate. Similar illumination pattern and Fourier transform could be obtained experimentally (Figure 1d, f). Furthermore, saturation would happen on both spatial and orientational dimension when saturated SIM[14] is performed. Higher-order spatial and orientational harmonics could further improve not only spatial resolution but also orientational resolution. Nonlinear orientational structured illumination also happens in the turning off process of nonlinear SIM with photoswitching proteins[15], whose first harmonics and second harmonics are measured by combination of polarized excitation and polarized detection experimentally (Figure S3).

Among all the promising findings based on spatial-orientational hyperspace, we focused on developing polarized SIM in this work, because it could be directly performed on any commercial SIM systems as well as most home-built SIM setups. To enable SIM with dipole orientation imaging, several problems need to be addressed. Firstly, the intensity fluctuation among different polarized excitations should be properly compensated, otherwise it would disturb the measurement of dipole orientation. In SIM, both the polarization and interferometric pattern are rotated, which can bring large heterogeneous intensity fluctuation, different from linear dichroism in which only the polarization is rotated. To calibrate the intensity fluctuation of different illumination patterns in SIM system, we used the specimen of sparsely distributed 100-nm fluorescent beads. The polarization-isotropic fluorescent beads emit constant fluorescence under different polarizations,

therefore fluctuation of their fluorescent signal reflects the intensity fluctuation of the system. We move the beads to cover the entire field of view for hundreds of measurements and generate the calibration map. According to our experimental results, the intensity fluctuation can be as large as 50% percent on a commercial GE OMX system, which would disrupt dipole orientation imaging if not compensated (Figure S4).

The next step is to solve the frequency components in Figure 1e. The spatial frequency components (marked in blue) could be solved as conventional SIM does (Eq. 3). Three interferometric directions would bring six detectable spatial pedals on the reciprocal space of PSIM. The orientational frequency components (marked in yellow) are solved using three polarizations (Eq. 4). Two orientational pedals could be obtained on the reciprocal space of PSIM. These pedals make up the detectable frequency region of PSIM in spatial-orientational k space (Figure 1g). Those spatial-orientational cross harmonics (marked in gray) could not be solved with commercial SIM setup, because excitation polarization θ and illumination vector \mathbf{k} are dependent on each other. However, these missing frequencies have no influence on either spatial image or dipole orientation image according to our simulation (Figure S5). Assembling all the frequency components of PSIM and applying inverse Fourier transform, super-resolution imaging of fluorescent dipoles could be achieved. The images are displayed in pseudo-color in HSV space, with fluorescent intensity and dipole orientation represented by value and hue correspondingly. An additional color wheel easily indicates the relationship between dipole orientation and color (Figure 2).

To verify our PSIM technique, we imaged phalloidin-Alexa 488 labeled actin in fixed BPAE cells, whose dipole orientations are well known. Considering the specimen in spatial-orientational hyperspace, PSIM extends SIM with dipole orientation imaging and reveals parallel dipole orientation of Alexa 488 to the filament direction (Figure 2a-b). Compared to linear dichroism with diffraction limited resolution, PSIM allows studying dipole orientations on individual filaments (Figure 2c-d). Integrated with 3D-SIM, PSIM could achieve optical sectioning and axial super-resolution as well, which enable us to image phalloidin-Alexa 568 labeled mouse kidney section with an axial range of 9 μm (Figure 2e-f). Removal of out-of-focus background is crucial for thick specimen and gives us a much clearer picture of the dipole distribution. Inherited from SIM, PSIM is very compatible with live cell imaging. Live cell imaging on GFP labeled lysosome and mitochondria in U2OS cells are also performed, as well as 3D PSIM imaging (Figure S6-7, Supplementary Movie 1-4).

Various super-resolution FPM techniques have been developed previously: (1) super resolution by polarization demodulation using linear dichroism[2, 3]; (2) Excitation Polarization Angle Narrowing (ExPAN) by STimulated Emission Depletion (STED)[2]; (3) single fluorescent dipole imaging by polarized STORM[10, 11, 16] or single dipole tracking[12, 17, 18]. PSIM achieves higher spatial resolution than polarization demodulation methods or ExPAN. Single molecular methods either take tens of minutes of imaging time which are not suitable for live cells, or only apply to sparsely labeled specimen[12, 17, 18]. Benefitted from its inherent super-resolution and orientation imaging capacities, PSIM can be an optimal method for live cell FPM imaging. Furthermore, the rapid progress in the development of SIM would also advance the performance of PSIM. For example, high-NA TIRF-SIM achieves a spatial resolution of 84-nm[19] and Hessian SIM achieves fast imaging speed of 188 Hz[20], both of which are well compatible with PSIM. With full compatibility to existing SIM systems, we believe PSIM to be a widely applied tool in studying molecular structure and dynamic in biology.

Methods

Reconstruction algorithm of PSIM. PSIM imaging process is described by Eq.1, whose Fourier transform would be:

$$\begin{aligned}\tilde{D}_{\theta,\phi}(\mathbf{k}_r, k_\alpha) &= [\tilde{S}_p(\mathbf{k}_r, k_\alpha) \otimes \tilde{I}_{\theta,\phi}(\mathbf{k}_r) \otimes \tilde{F}_\theta(k_\alpha)] \cdot OTF(\mathbf{k}_r, k_\alpha) \\ \tilde{I}_{\theta,\phi}(\mathbf{k}_r) &= \frac{\pi I_0}{4} [\delta(\mathbf{k}_r) + \frac{1}{2} e^{i\phi} \delta(\mathbf{k}_r - \mathbf{k}_\theta) + \frac{1}{2} e^{-i\phi} \delta(\mathbf{k}_r + \mathbf{k}_\theta)] \\ \tilde{F}_\theta(k_\alpha) &= \frac{\pi \eta}{4} [\delta(k_\alpha) + \frac{1}{2} e^{-2i\theta} \delta(k_\alpha - \frac{1}{\pi}) + \frac{1}{2} e^{2i\theta} \delta(k_\alpha + \frac{1}{\pi})]\end{aligned}\quad (2)$$

Both the spatial structured illumination, $I_{\theta,\phi}(\mathbf{r})$ and orientational structured illumination $F_\eta(\alpha)$ bring larger observable region on spatial dimensions and orientational dimension. The reconstruction of PSIM takes two steps: SIM step and LD step. For SIM step, three images belong to the same pattern are used to solve the three frequency components as conventional SIM does. However, every frequency component is convoluted with a polarization term $\tilde{F}_\theta(k_\alpha)$, as shown in Eq. 3

$$\begin{aligned}\begin{bmatrix} \tilde{D}_{\theta_i,\phi_1}(\mathbf{k}_r, k_\alpha) \\ \tilde{D}_{\theta_i,\phi_2}(\mathbf{k}_r, k_\alpha) \\ \tilde{D}_{\theta_i,\phi_3}(\mathbf{k}_r, k_\alpha) \end{bmatrix} &= M_{SIM} \cdot \begin{bmatrix} [\tilde{S}_p(\mathbf{k}_r, k_\alpha) \otimes \tilde{F}_{\theta_i}(k_\alpha)] \cdot OTF(\mathbf{k}_r, k_\alpha) \\ [\tilde{S}_p(\mathbf{k}_r - \mathbf{k}_{\theta_i}, k_\alpha) \otimes \tilde{F}_{\theta_i}(k_\alpha)] \cdot OTF(\mathbf{k}_r, k_\alpha) \\ [\tilde{S}_p(\mathbf{k}_r + \mathbf{k}_{\theta_i}, k_\alpha) \otimes \tilde{F}_{\theta_i}(k_\alpha)] \cdot OTF(\mathbf{k}_r, k_\alpha) \end{bmatrix}; \\ M_{SIM} &= \frac{\pi I_0}{4} \begin{bmatrix} 1 & \frac{1}{2} e^{i\phi_1} & \frac{1}{2} e^{+i\phi_1} \\ 1 & \frac{1}{2} e^{i\phi_2} & \frac{1}{2} e^{+i\phi_2} \\ 1 & \frac{1}{2} e^{i\phi_3} & \frac{1}{2} e^{+i\phi_3} \end{bmatrix}\end{aligned}\quad (3)$$

Then LD step follows. From the 3 original spatial components $\tilde{S}_p(\mathbf{k}_r, k_\alpha) \otimes \tilde{F}_{\theta_i}(k_\alpha)$, ($i = 1, 2, 3$), $\tilde{S}_p(\mathbf{k}_r, k_\alpha)$, $\tilde{S}_p(\mathbf{k}_r, k_\alpha - \frac{1}{\pi})$, $\tilde{S}_p(\mathbf{k}_r, k_\alpha + \frac{1}{\pi})$ could be further solved with LD equation (Eq. 4). SIM uses 3 directions of illumination patterns, which cover the doubled region in reciprocal space. The 3 directions of polarization are just sufficient to extract the dipole orientations, while LD systems usually use more excitation polarizations to obtain robust results. Before the LD step, the images are compensated with the calibration data of fluorescent beads.

$$\begin{aligned}\begin{bmatrix} \tilde{S}_p(\mathbf{k}_r, k_\alpha) \otimes \tilde{F}_{\theta_1}(k_\alpha) \\ \tilde{S}_p(\mathbf{k}_r, k_\alpha) \otimes \tilde{F}_{\theta_2}(k_\alpha) \\ \tilde{S}_p(\mathbf{k}_r, k_\alpha) \otimes \tilde{F}_{\theta_3}(k_\alpha) \end{bmatrix} &= M_{LD} \cdot \begin{bmatrix} \tilde{S}_p(\mathbf{k}_r, k_\alpha) \cdot OTF(\mathbf{k}_r, k_\alpha) \\ \tilde{S}_p(\mathbf{k}_r, k_\alpha - \frac{1}{\pi}) \cdot OTF(\mathbf{k}_r, k_\alpha) \\ \tilde{S}_p(\mathbf{k}_r, k_\alpha + \frac{1}{\pi}) \cdot OTF(\mathbf{k}_r, k_\alpha) \end{bmatrix}; \\ M_{LD} &= \frac{\pi \eta}{4} \begin{bmatrix} 1 & \frac{1}{2} e^{-i2\theta_1} & \frac{1}{2} e^{+i2\theta_1} \\ 1 & \frac{1}{2} e^{-i2\theta_2} & \frac{1}{2} e^{+i2\theta_2} \\ 1 & \frac{1}{2} e^{-i2\theta_3} & \frac{1}{2} e^{+i2\theta_3} \end{bmatrix}\end{aligned}\quad (4)$$

These 3 components solved in LD step, together with other 6 components ($\tilde{S}_p(\mathbf{k}_r \pm \mathbf{k}_{\theta_i}, k_\alpha) \otimes \tilde{F}_{\theta_i}(k_\alpha)$, $i = 1, 2, 3$) solved in SIM step make up the observable region of reciprocal space of PSIM (Figure 1g). The 6 high-order spatial components ($\tilde{S}_p(\mathbf{k}_r \pm \mathbf{k}_{\theta_i}, k_\alpha) \otimes \tilde{F}_{\theta_i}(k_\alpha)$, $i = 1, 2, 3$) couldnt be further solved to get separated polarization components $\tilde{S}_p(\mathbf{k}_r \pm \mathbf{k}_{\theta_i}, k_\alpha)$ and $\tilde{S}_p(\mathbf{k}_r \pm \mathbf{k}_{\theta_i}, k_\alpha \pm \frac{1}{\pi})$, $i = 1, 2, 3$ (cross first harmonics). Assembling the 9 shifted components in reciprocal space and applying inverse Fourier transform on spatial dimensions. The intensity image could be obtained from the zero frequency component on orientation axis. And the dipole orientation could be obtained from the phase of +1 harmonic on orientation axis.

Our SIM reconstruction algorithm is based on previous work of fairSIM (<https://www.fairsim.org/>)[21], which is an ImageJ plugin written in Java. However, our data is analyzed by reprogrammed

Matlab code for easier debugging. A simple ImageJ plugin has also been developed for user-friendly operation. To facilitate the science community, we have released our source code on Github (<https://github.com/chenxy2012/PSIM>).

Calibration of illumination fluctuation. The slide of 100 nm fluorescent beads is prepared at a proper density so that the beads can be localized separately. The beads are imaged by 2D-SIM sequence at largest field-of-view of the system. For each pattern, three images of different phase are acquired, from which the wide field image can be calculated. If the phase difference is designed to be $2\pi/3$, wide field image could be easily obtained by averaging the three images. Thus, three wide field images are obtained for three patterns. In each image, the beads are localized by QuickPALM (<http://code.google.com/p/quickpalm>)[22] with their position and intensity exported. For those beads appears on all three images at the same position, they are used to compensate illumination fluctuations among different patterns. The beads are then moved at a step size of 500 nm and measured repeatedly until the whole field-of-view is calibrated. Compensation of intensity fluctuation is performed before the LD step during PSIM reconstruction based on Eq. 5. Detailed information is included in Supplementary Note 4.

$$\begin{aligned} D &= (S \cdot Calib) \otimes PSF \\ D_{calib} &= F^{-1}\{F\{D\}/OTF\}/Calib \end{aligned} \quad (5)$$

Simulations to verify PSIM. The spatial-orientational cross harmonic frequency components are unresolvable by PSIM, so that PSIM uses the obtained 9 frequency pedals to generate dipole orientation image. If all the components are solved separately, 21 frequency pedals are obtained to fill up the full doubled region (Figure S5). To study the influence of missing cross harmonic frequencies, we simulated radial lines and circles with parallel dipole orientation to their direction. The simulated specimen in x - y - α coordinate is discretized with spatial grid of 20 nm and orientational grid of 12.5 degree. Then we apply Fourier transform to the simulated data and obtain corresponding frequency pedals. Frequency components beyond the observable area of PSIM (Figure 1g) or full double region (Figure S5a) are neglected. Afterward, inverse Fourier transform is applied and super-resolution dipole imaging is obtained. We find that the missing frequency components have no influence on either intensity image or dipole orientations. They only have influence on the orientation uniform factor (OUF)[3], which describes the variation of dipole orientations or wobbling of dipoles on each pixel. Unexpected high-frequency fluctuations would appear on the OUF image. The edges of filaments show highest OUF while the filaments themselves have small OUF (Figure S5e).

Experimental measurement of structured illumination. A single-layer uniform 20 nm fluorescent beads sample is prepared to measure the spatial-orientational structured illumination, which is excited by an interferometric structured illumination. Polarization detection is implemented by placing a polarizer in front of the detector. The polarizer rotates from 0 to 180 degrees and images are captured every 20 degrees. So nine images with the same spatial pattern but different polarized detections are acquired under this configuration. After that, all images are rotated for the same angle to make the stripes vertical. Afterward, columns of the image are averaged to form a row as a spatial dimension. Then nine polarized detections are placed in a columns form the orientational dimension (Figure 1d). Finally, the frequency domain of the structured illumination in spatial-orientational hyperspace is acquired by 2D Fourier Transform (Figure 1f).

Sample preparation and imaging. The sample of Alexa-488 Phalloidin labeled F-actin in BAPE cell and Alexa-568 Phalloidin labeled actin in mouse kidney section are purchased from ThermoFisher (FluoCells Prepared Slide #1 and FluoCells Prepared Slide #3). SIM imaging was performed on a commercial system (DeltaVision OMX SR, GE, US), with 60X 1.4 NA oil immersion

objective (Olympus, Japan) and AF488/AF561 filter sets. Standard 2D SIM or 3D SIM sequence was performed 285 with 80 nm pixel size and 125 nm axial step.

Data availability. The data that support the findings of this study are available from the corresponding authors upon reasonable request.

Author Contributions

PX and QD supervised the research. KZ and PX designed the experiments. XC and KZ programmed PSIM algorithm and analyzed the data. WL, ML, and KZ experimentally measured the illumination pattern of linear and nonlinear PSIM. KZ, PX, and XC wrote the manuscript with inputs from all authors.

Acknowledgments

This work was supported by the National Key Research and Development Program of China (2017YFC0110202), the National Instrument Development Special Program (2013YQ03065102), the National Natural Science Foundation of China (61475010, 61729501, 61327902). We thank the Core Facilities of Life Sciences, Peking University for assistance with SIM Imaging.

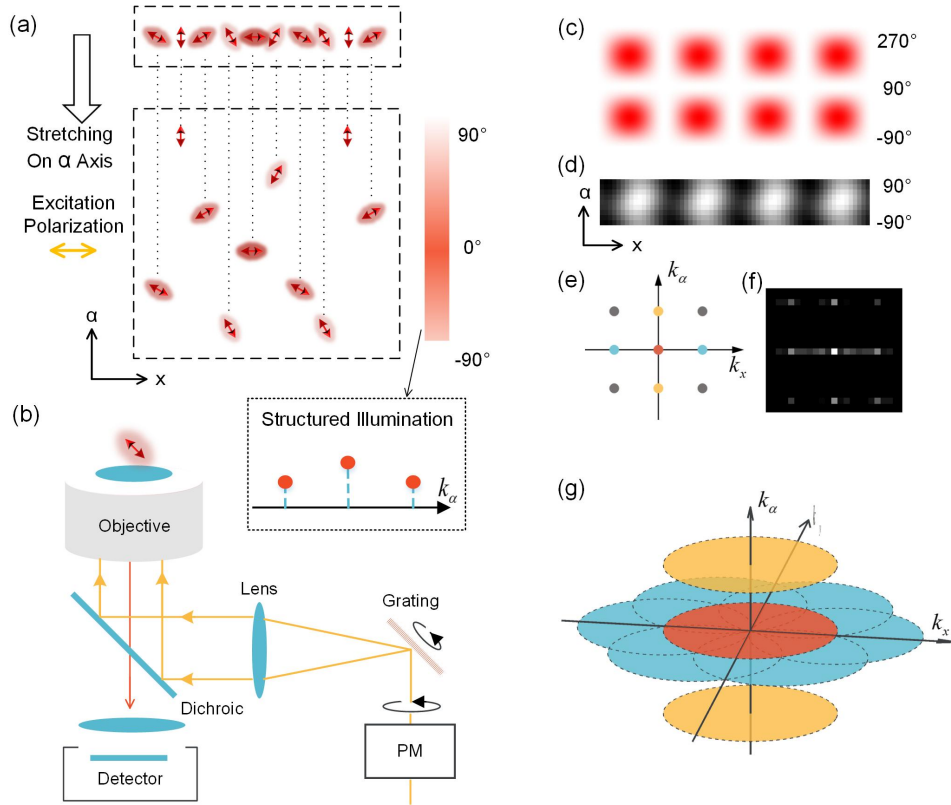


Figure 1: **Illustration of spatial-orientational hyperspace.** (a) Taking the fluorescent dipoles in spatial-orientational hyperspace, excitation of a linearly polarized laser achieves similar sinusoidal illumination on orientation dimension, whose Fourier transform contains three frequency components. (b) In SIM setup, the grating generates multiple laser beams for interference. A polarization modulation (PM) module synchronizes the polarization with the rotation of gratings. The interferometric pattern of s-polarized lasers achieves highest contrast. (c) The x - α section of spatial-orientational structured illumination is displayed, since the illumination along y -axis is uniform. (d) Experimentally measured 2D pattern of structured illumination in x - α coordinate. (e) Fourier transform of the 2D pattern brings spatial harmonics (blue), orientational harmonics (yellow), and cross harmonics (gray). (f) Fourier transform of the experimental structured illumination in (d). (g) Observable region of PSIM in frequency domain, which is expanded on both spatial and orientational dimension.

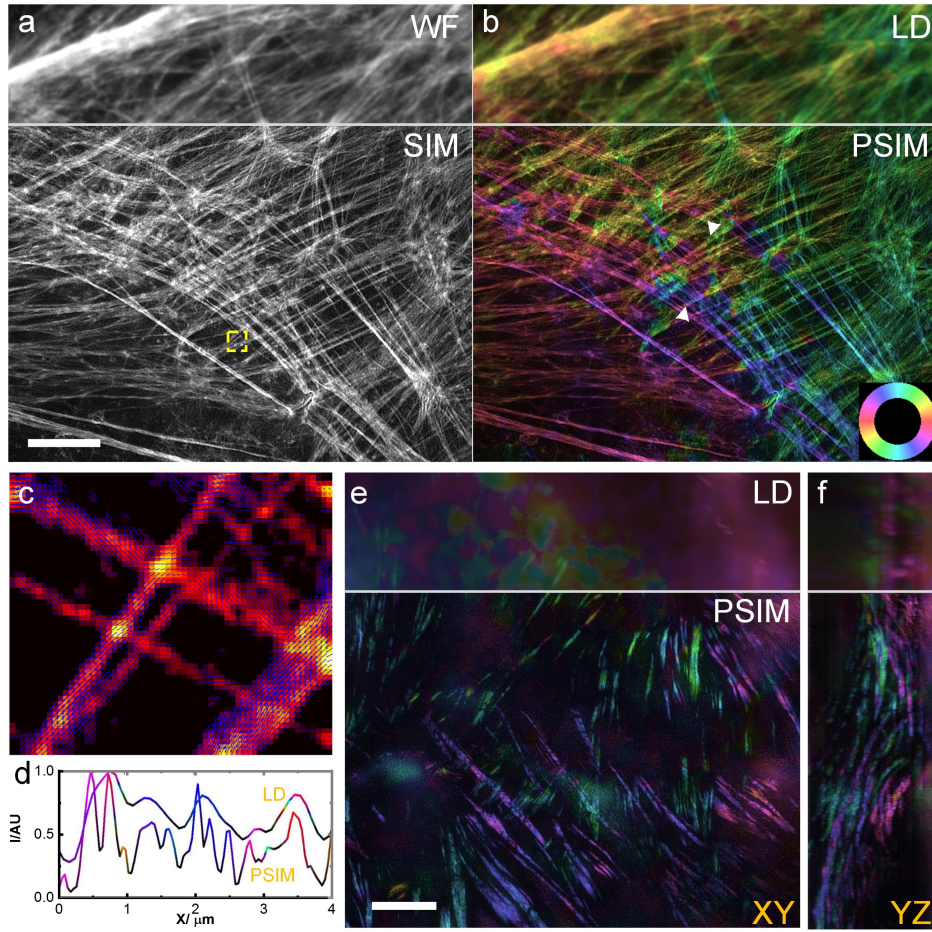


Figure 2: **PSIM imaging results.** (a, b) Phalloidin-Alexa 488 labeled actin in BPAE cells is imaged by 2D-PSIM. (a) When only spatial dimension considered, the intensity image is obtained, in which the upper part is diffraction-limited and the lower part is super-resolved. (b) When the specimen is considered in spatial-orientational hyperspace, the dipole orientations are additionally measured and marked with pseudo-color. The lower part is PSIM result, which achieves super-resolution compared to LD and obtain dipole orientations compared to SIM. The relationship between pseudo-color and dipole orientation is indicated by a color wheel on bottom-right corner. (c) Magnified view of the boxed region in (a) with the dipole orientations shown by the blue arrows. (d) Intensity profile of LD and PSIM between the two arrows in (b), with pseudo-color indicating their corresponding dipole orientation. PSIM reveals the dipole orientation on individual actin filaments. (e, f) Phalloidin-Alexa 561 labeled actin in mouse kidney section is imaged by 3D-PSIM. Max Intensity Projection (MIP) imaged on XY plane and YZ plane are included. 3D-PSIM (lower part of e, f) removes most of out-of-focus background compared to linear dichroism (upper part of e, f). The pseudo-color used in b, d, e, f shares the same color-wheel. Scale bar: $5 \mu m$.

REFERENCES

- [1] Kim I Mortensen, L Stirling Churchman, James A Spudich, and Henrik Flyvbjerg. Optimized localization analysis for single-molecule tracking and super-resolution microscopy. *Nature methods*, 7(5):377, 2010.
- [2] Nour Hafi, Matthias Grunwald, Laura S Van Den Heuvel, Timo Aspelmeier, Jian-Hua Chen, Marta Zagrebelsky, Ole M Schütte, Claudia Steinem, Martin Korte, Axel Munk, et al. Fluorescence nanoscopy by polarization modulation and polarization angle narrowing. *Nature methods*, 11(5):579, 2014.
- [3] Karl Zhanghao, Long Chen, Xu-San Yang, Miao-Yan Wang, Zhen-Li Jing, Hong-Bin Han, Michael Q Zhang, Dayong Jin, Jun-Tao Gao, and Peng Xi. Super-resolution dipole orientation mapping via polarization demodulation. *Light: Science & Applications*, 5(10):e16166, 2016.
- [4] David Artigas, David Merino, Christoph Polzer, and Pablo Loza-Alvarez. Sub-diffraction discrimination with polarization-resolved two-photon excited fluorescence microscopy. *Optica*, 4(8):911–918, 2017.
- [5] Josef Lazar, Alexey Bondar, Stepan Timr, and Stuart J Firestein. Two-photon polarization microscopy reveals protein structure and function. *Nature methods*, 8(8):684, 2011.
- [6] Martin Kampmann, Claire E Atkinson, Alexa L Mattheyses, and Sanford M Simon. Mapping the orientation of nuclear pore proteins in living cells with polarized fluorescence microscopy. *Nature Structural and Molecular Biology*, 18(6):643, 2011.
- [7] Takayuki Nishizaka, Kazuhiro Oiwa, Hiroyuki Noji, Shigeki Kimura, Eiro Muneyuki, Masasuke Yoshida, and Kazuhiko Kinoshita Jr. Chemomechanical coupling in f 1-atpase revealed by simultaneous observation of nucleotide kinetics and rotation. *Nature Structural and Molecular Biology*, 11(2):142, 2004.
- [8] Joseph N Forkey, Margot E Quinlan, M Alexander Shaw, John ET Corrie, and Yale E Goldman. Three-dimensional structural dynamics of myosin v by single-molecule fluorescence polarization. *Nature*, 422(6930):399, 2003.
- [9] Alina M Vrabioiu and Timothy J Mitchison. Structural insights into yeast septin organization from polarized fluorescence microscopy. *Nature*, 443(7110):466, 2006.
- [10] Adam S Backer, Maurice Y Lee, and WE Moerner. Enhanced dna imaging using super-resolution microscopy and simultaneous single-molecule orientation measurements. *Optica*, 3(6):659–666, 2016.
- [11] Cesar Augusto Valades Cruz, Haitham Ahmed Shaban, Alla Kress, Nicolas Bertaux, Serge Monneret, Manos Mavrikis, Julien Savatier, and Sophie Basselet. Quantitative nanoscale imaging of orientational order in biological filaments by polarized superresolution microscopy. *Proceedings of the National Academy of Sciences*, 113(7):E820–E828, 2016.
- [12] Shalin B Mehta, Molly McQuilken, Patrick J La Riviere, Patricia Occhipinti, Amitabh Verma, Rudolf Oldenbourg, Amy S Gladfelter, and Tomomi Tani. Dissection of molecular assembly dynamics by tracking orientation and position of single molecules in live cells. *Proceedings of the National Academy of Sciences*, 113(42):E6352–E6361, 2016.

- [13] Deborah Y Shroder, Lisa G Lippert, and Yale E Goldman. Single molecule optical measurements of orientation and rotations of biological macromolecules. *Methods and applications in fluorescence*, 4(4):042004, 2016.
- [14] Mats GL Gustafsson. Nonlinear structured-illumination microscopy: wide-field fluorescence imaging with theoretically unlimited resolution. *Proceedings of the National Academy of Sciences of the United States of America*, 102(37):13081–13086, 2005.
- [15] E Hesper Rego, Lin Shao, John J Macklin, Lukman Winoto, Göran A Johansson, Nicholas Kamps-Hughes, Michael W Davidson, and Mats GL Gustafsson. Nonlinear structured-illumination microscopy with a photoswitchable protein reveals cellular structures at 50-nm resolution. *Proceedings of the National Academy of Sciences*, 109(3):E135–E143, 2012.
- [16] Travis J Gould, Mudalige S Gunewardene, Manasa V Gudheti, Vladislav V Verkhusha, Shu-Rong Yin, Julie A Gosse, and Samuel T Hess. Nanoscale imaging of molecular positions and anisotropies. *Nature methods*, 5(12):1027, 2008.
- [17] Mikael P Backlund, Matthew D Lew, Adam S Backer, Steffen J Sahl, Ginni Grover, Anurag Agrawal, Rafael Piestun, and WE Moerner. Simultaneous, accurate measurement of the 3d position and orientation of single molecules. *Proceedings of the National Academy of Sciences*, 109(47):19087–19092, 2012.
- [18] Erdal Toprak, Joerg Enderlein, Sheyum Syed, Sean A McKinney, Rolfe G Petschek, Taekjip Ha, Yale E Goldman, and Paul R Selvin. Defocused orientation and position imaging (dopi) of myosin v. *Proceedings of the National Academy of Sciences*, 103(17):6495–6499, 2006.
- [19] Dong Li, Lin Shao, Bi-Chang Chen, Xi Zhang, Mingshu Zhang, Brian Moses, Daniel E Milkie, Jordan R Beach, John A Hammer, Mithun Pasham, et al. Extended-resolution structured illumination imaging of endocytic and cytoskeletal dynamics. *Science*, 349(6251):aab3500, 2015.
- [20] Xiaoshuai Huang, Junchao Fan, Liuju Li, Haosen Liu, Runlong Wu, Yi Wu, Lisi Wei, Heng Mao, Amit Lal, Peng Xi, et al. Fast, long-term, super-resolution imaging with hessian structured illumination microscopy. *Nature biotechnology*, 36(5):451, 2018.
- [21] Marcel Müller, Viola Mönkemöller, Simon Hennig, Wolfgang Hübner, and Thomas Huser. Open-source image reconstruction of super-resolution structured illumination microscopy data in imagej. *Nature communications*, 7:10980, 2016.
- [22] Ricardo Henriques, Mickael Lelek, Eugenio F Fornasiero, Flavia Valtorta, Christophe Zimmer, and Musa M Mhlanga. Quickpalm: 3d real-time photoactivation nanoscopy image processing in imagej. *Nature methods*, 7(5):339, 2010.